REVISED MANUSCRIPT

ELECTRONIC SUPPLEMENTARY INFORMATION

Mono- and Binuclear Chiral N,N,O-Scorpionate Zinc Alkyls as Efficient Initiators for the ROP of *rac*-Lactide.

Antonio Otero,[*,a] *Juan Fernández-Baeza,*[*,a] *Luis F. Sánchez-Barba,*[*,b] *Sonia Sobrino,*[a] *Andrés Garcés,*[b] *Agustín Lara-Sánchez,*[a] *and Ana M. Rodríguez*[a]

[a]Prof. Dr. Antonio Otero, Dr. Juan Fernández-Baeza, Dña. Sonia Sobrino Dr Agustín Lara-Sánchez, Dr. Ana M. Rodríguez.

Universidad de Castilla-La Mancha, Departamento de Química Inorgánica, Orgánica y Bioquímica-Centro de Innovación en Química Avanzada (ORFEO-CINQA), Campus Universitario, 13071-Ciudad Real, Spain.

E-mail: antonio.otero@uclm.es; juan.fbaeza@uclm.es;

[b]Dr. Luis F. Sánchez-Barba, Dr. Andrés Garcés.

Universidad *Rey Juan Carlos, Departamento de Biología y Geología, Física y Química Inorgánica, Móstoles-28933-Madrid, Spain.*

E-mail: luisfernando.sanchezbarba@urjc.es

Table of Contents

1) NMR characterization for complexes **1**-**3**, **4**, **7**, **10**, **13**, **15** and **17**:

Figure S1-S9. ^{1}H and $^{13}C\{^{1}H\}$ NMR spectra……..……S4

2) Dynamic behavior studies:

Figure S10. ^{1}H NMR spectrum for complex **13** at 25 and 60ºC in thf-d_8……..…...…...…….....……S13

Figure S11. ^{1}H NMR spectrum for complex **13** and $ZnMe_2$ at 25ºC in thf-d_8…….……...…...…….....……S14

3) Ring-opening polymerization of *rac*-lactide details:

Figure S12. GPC trace corresponding to a poly(*rac*-lactide) sample……..……...…….S15

Figure S13. Plot of PLA M_n and molecular weight distribution values (PDI) as a function of monomer conversion (%) employing **7**……..……...……...…...…S16

Figure S14. Selected area of MALDI-ToF mass spectra of poly(*rac*-lactide) synthesized using initiators **7** and **8**…….....……..……..……...S17

Figure S15. Pseudo-first-order kinetic plots for *rac*-LA polymerizations employing **7**…..….S19

Figure S16. Plots of ln k_{app} versus ln $[catalyst]_0$ for the polymerization of *rac*-LA employing **7**……..……....S20

Table S1. Rate constants dependence on the initial catalyst concentration for **7**.....S21

Figure S17. ^{1}H NMR spectrum of poly(*rac*-lactide) showing the chain-end *termini*.....S22

Figure S18. ^{1}H NMR spectrum of the homodecoupled C*H* resonance of poly(*rac*-lactide) prepared from catalyst **6**…….……...…….....…….S23

4) X-ray diffraction experimental details:

Table S2. Crystal data and structure refinement for **4** and **5**…….S24

5) References……..…….…….....……S25

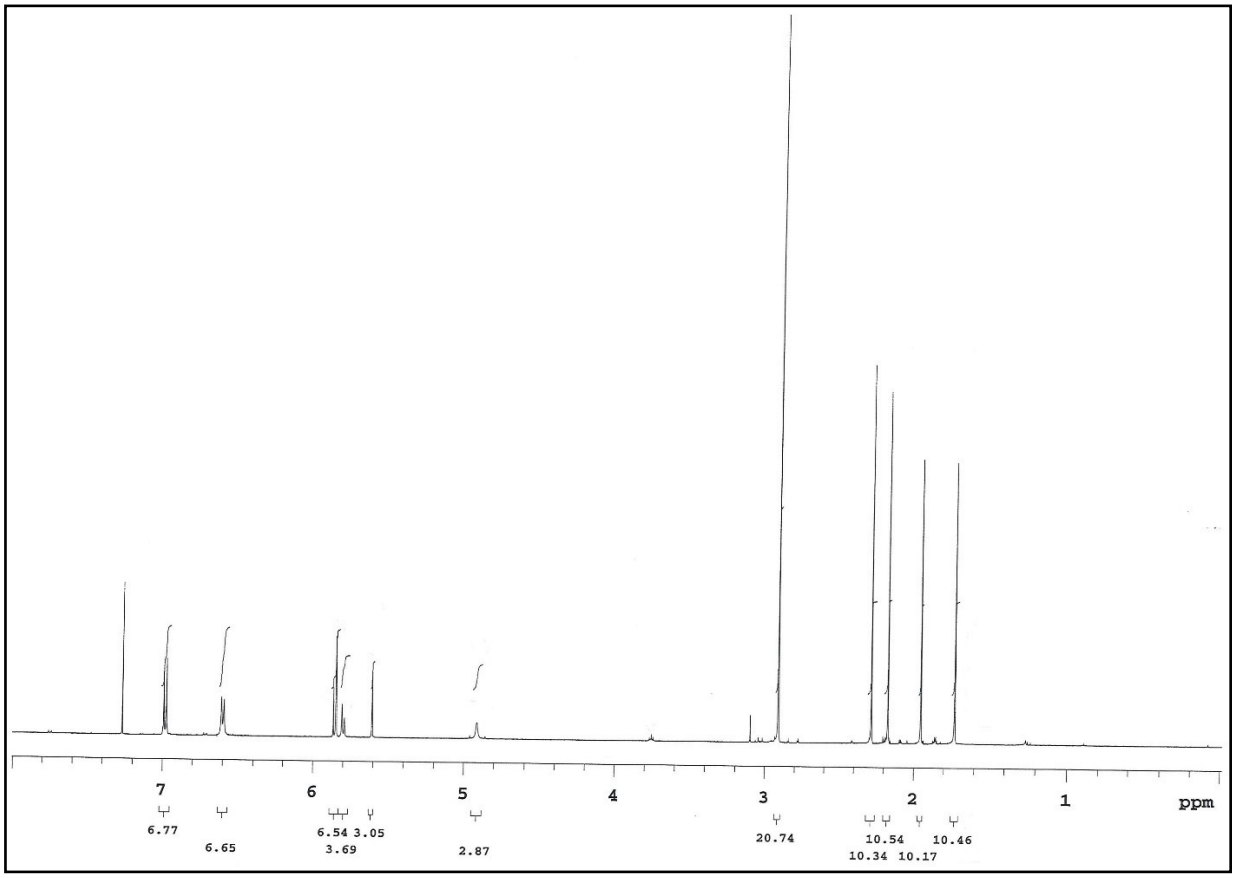

Figure S1a. ^{1}H NMR spectrum of compound bpzampeH (**1**).

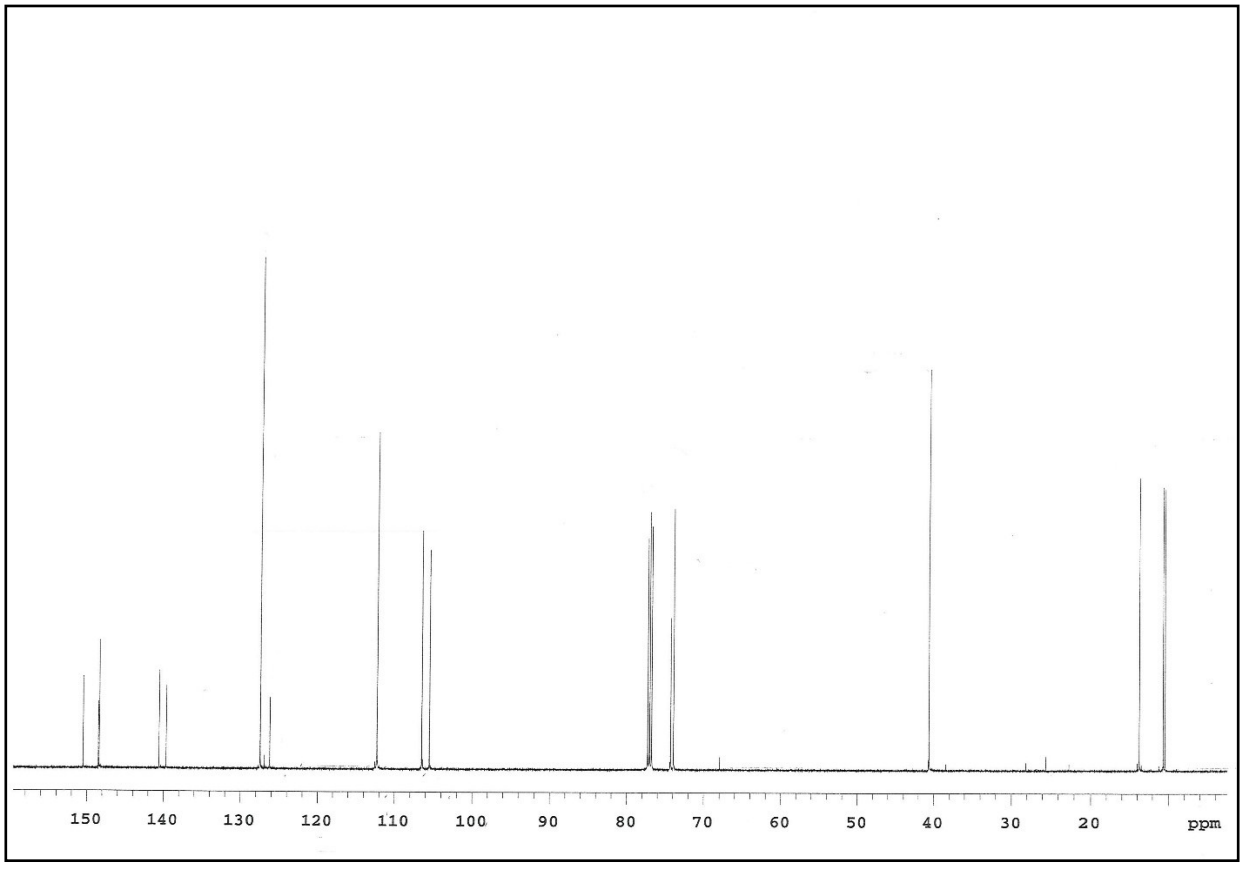

Figure S1b. ^{13}C{^{1}H} NMR spectrum of compound bpzampeH (**1**).

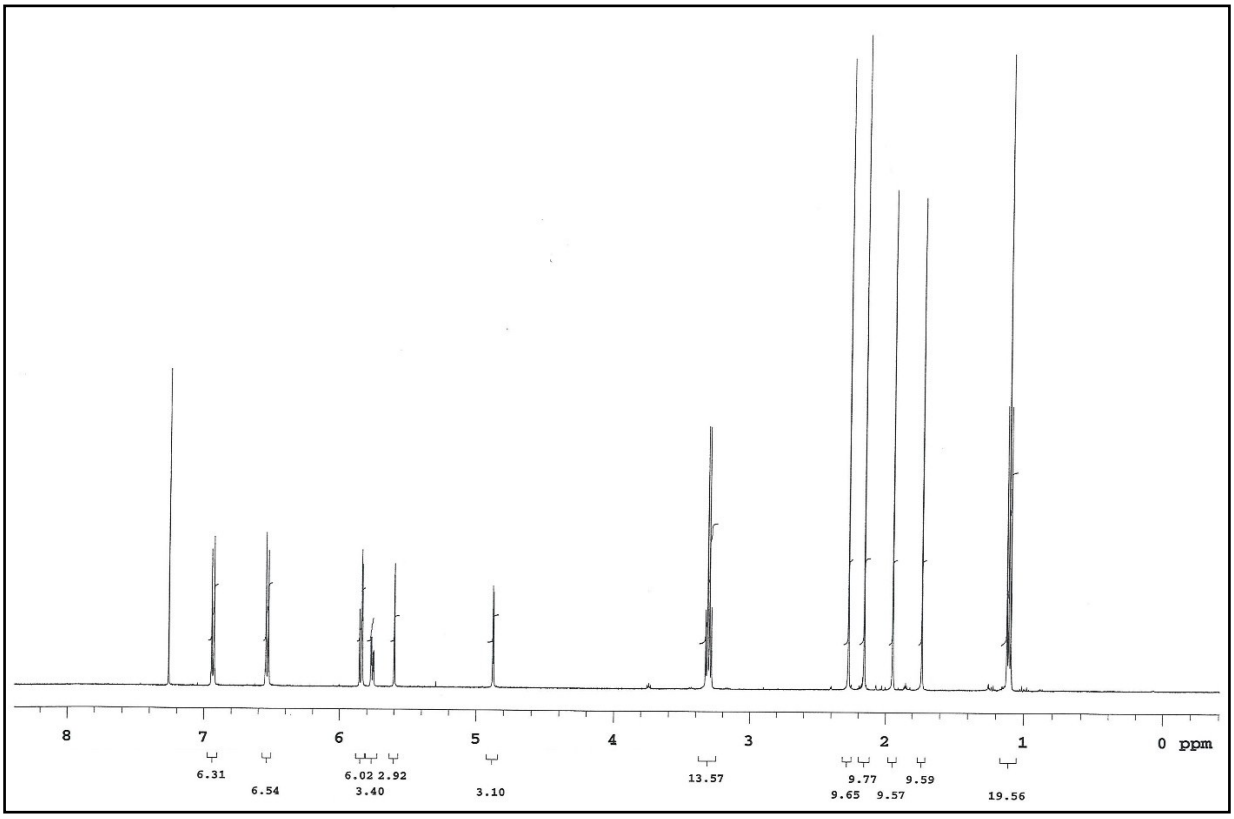

Figure S2a. ^{1}H NMR spectrum of compound bpzaepeH (**2**).

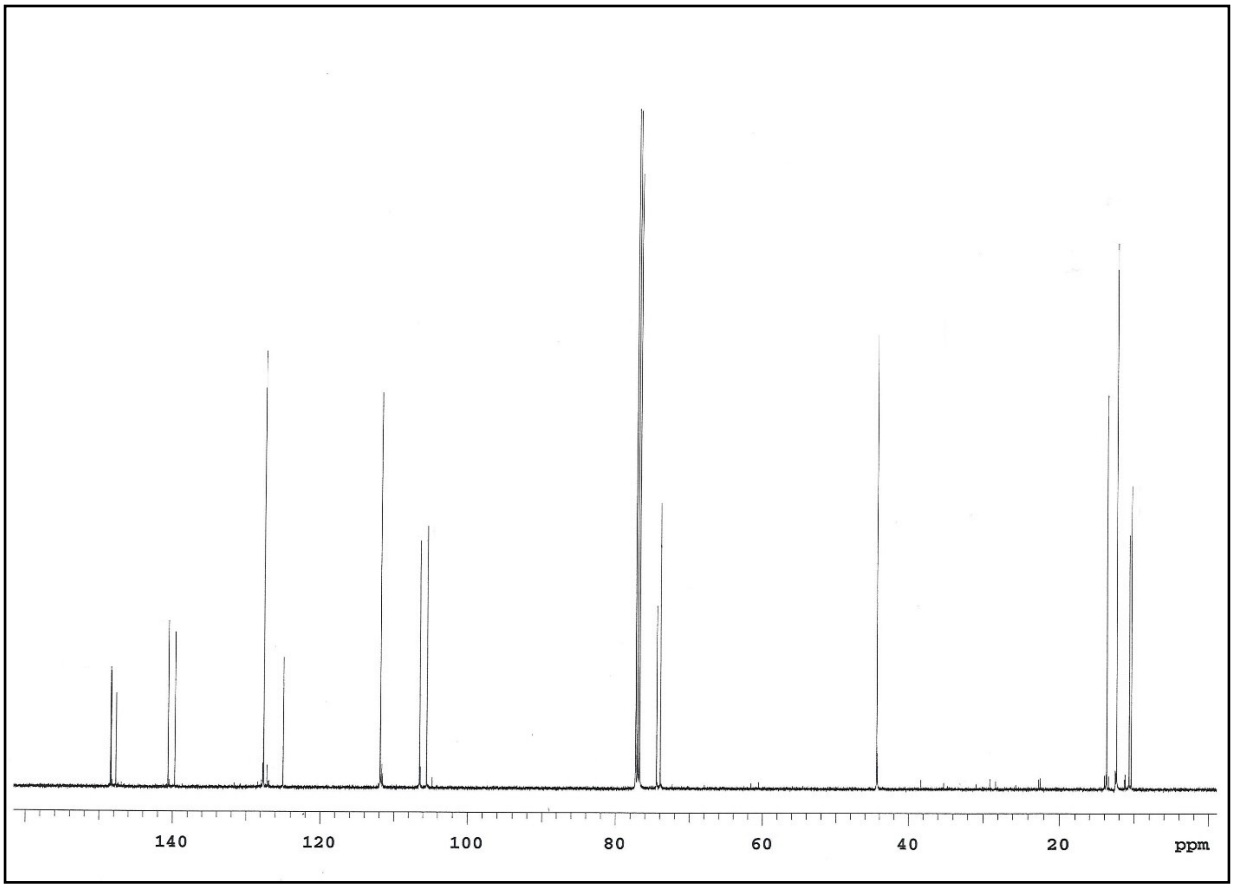

Figure S2b. $^{13}C\{^{1}H\}$ NMR spectrum of compound bpzaepeH (**2**).

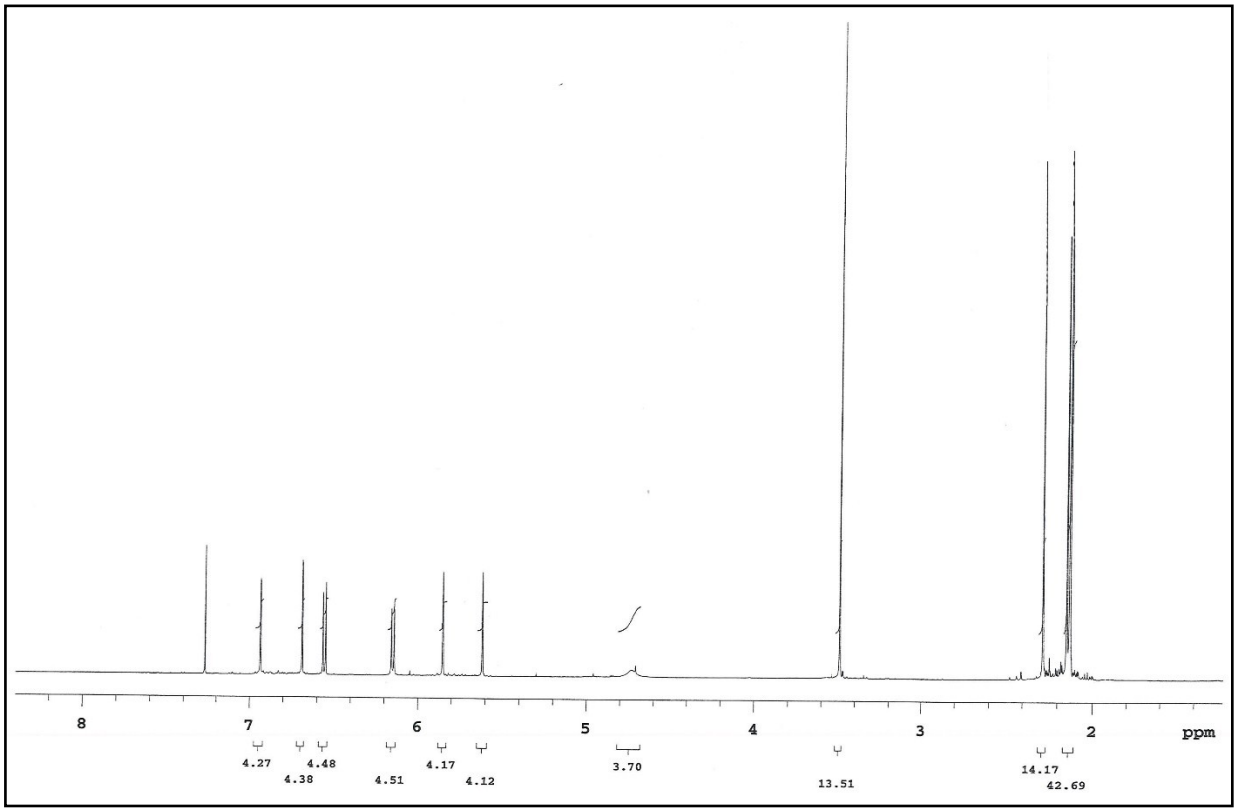

Figure S3a. ^{1}H NMR spectrum of compound bpzimeH (**3**).

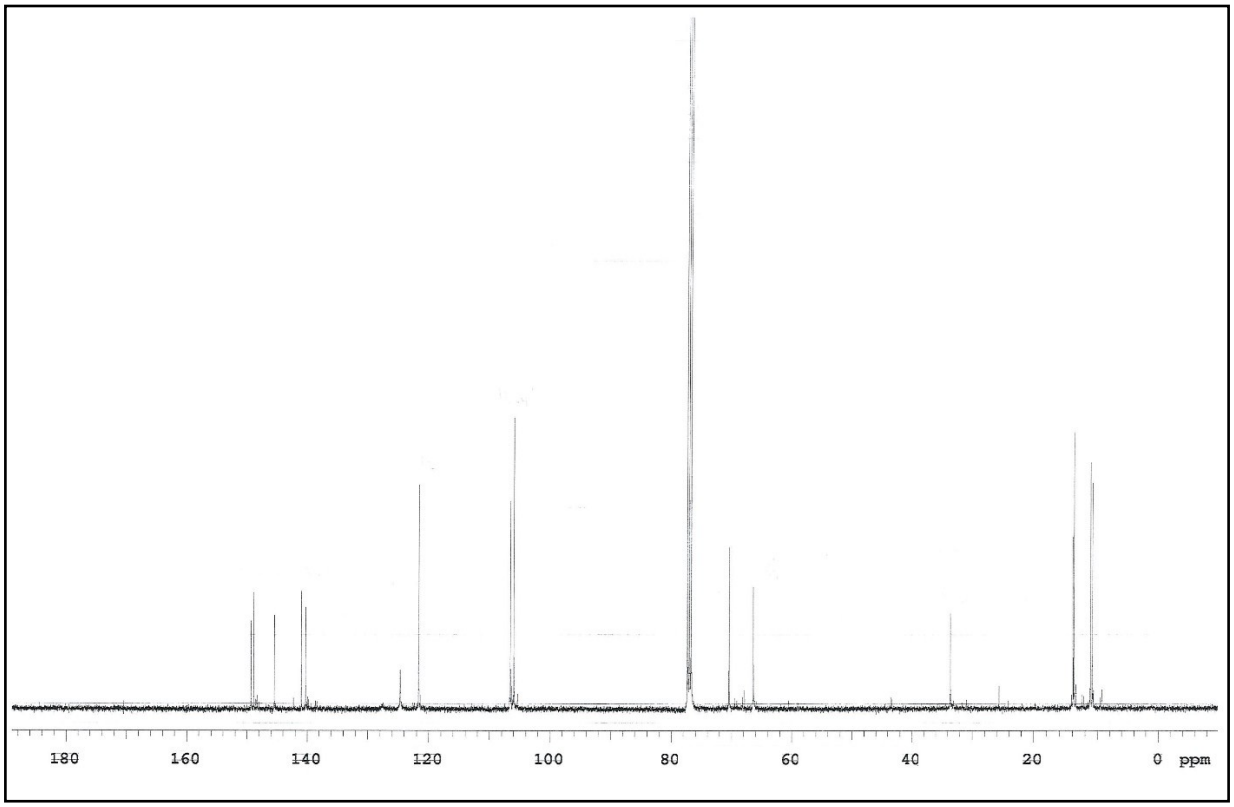

Figure S3b. $^{13}C\{^{1}H\}$ NMR spectrum of compound bpzimeH (**3**).

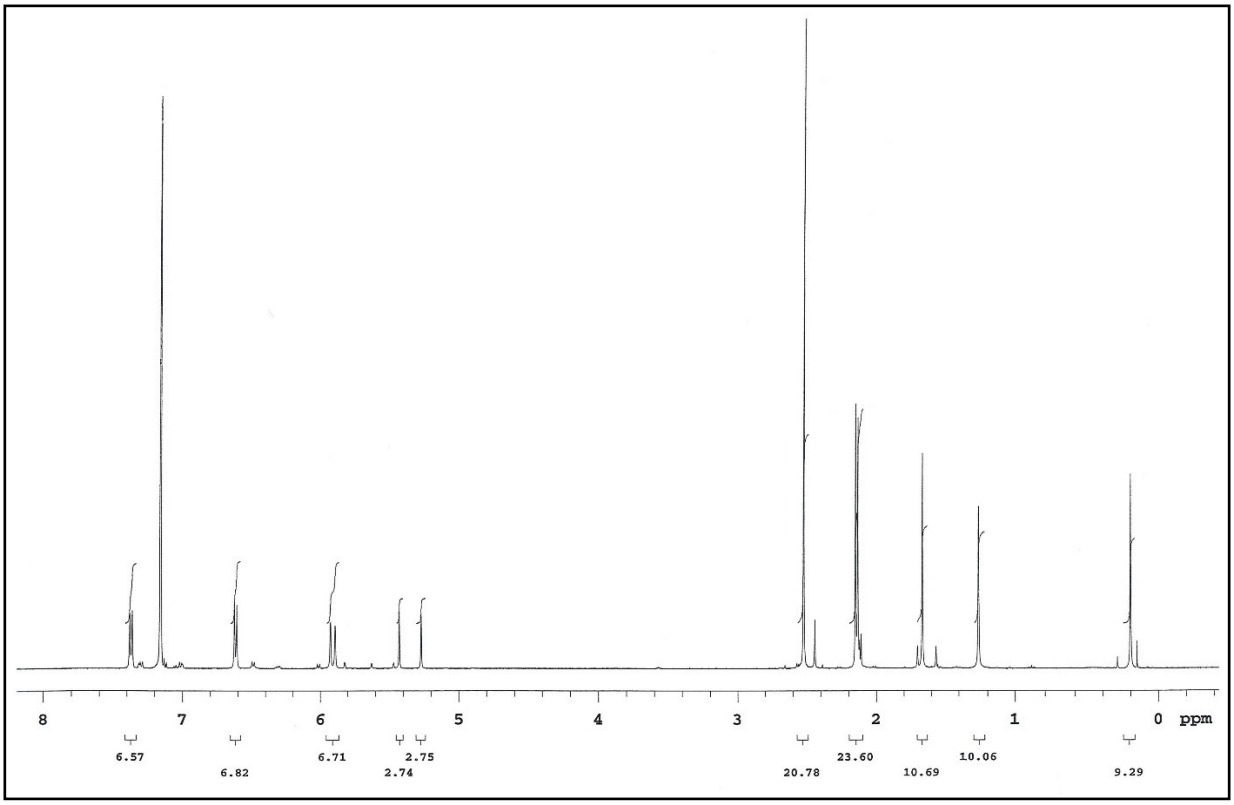

Figure S4a. ^{1}H NMR spectrum of complex [Zn(Me)(bpzampe)] (**4**).

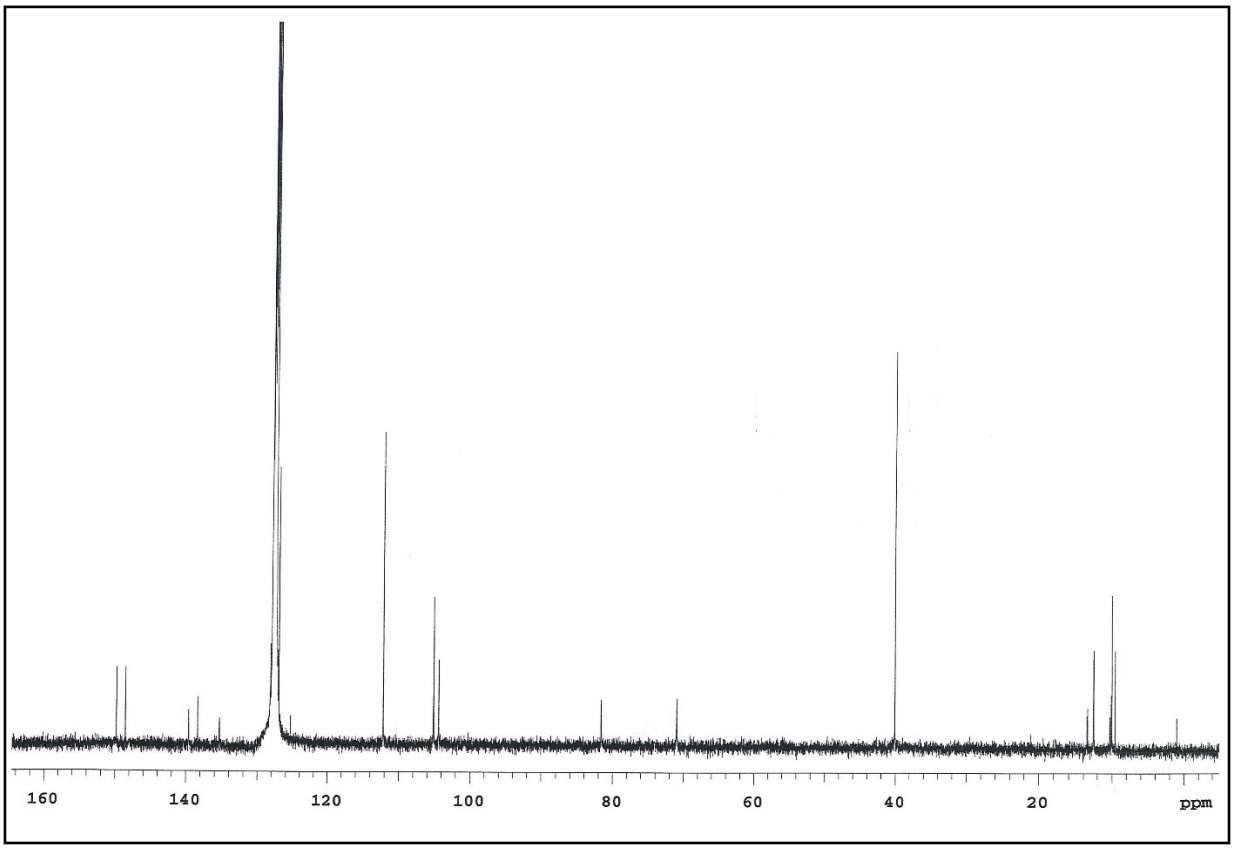

Figure S4b. $^{13}C\{^{1}H\}$ NMR spectrum of complex [Zn(Me)(bpzampe)] (**4**).

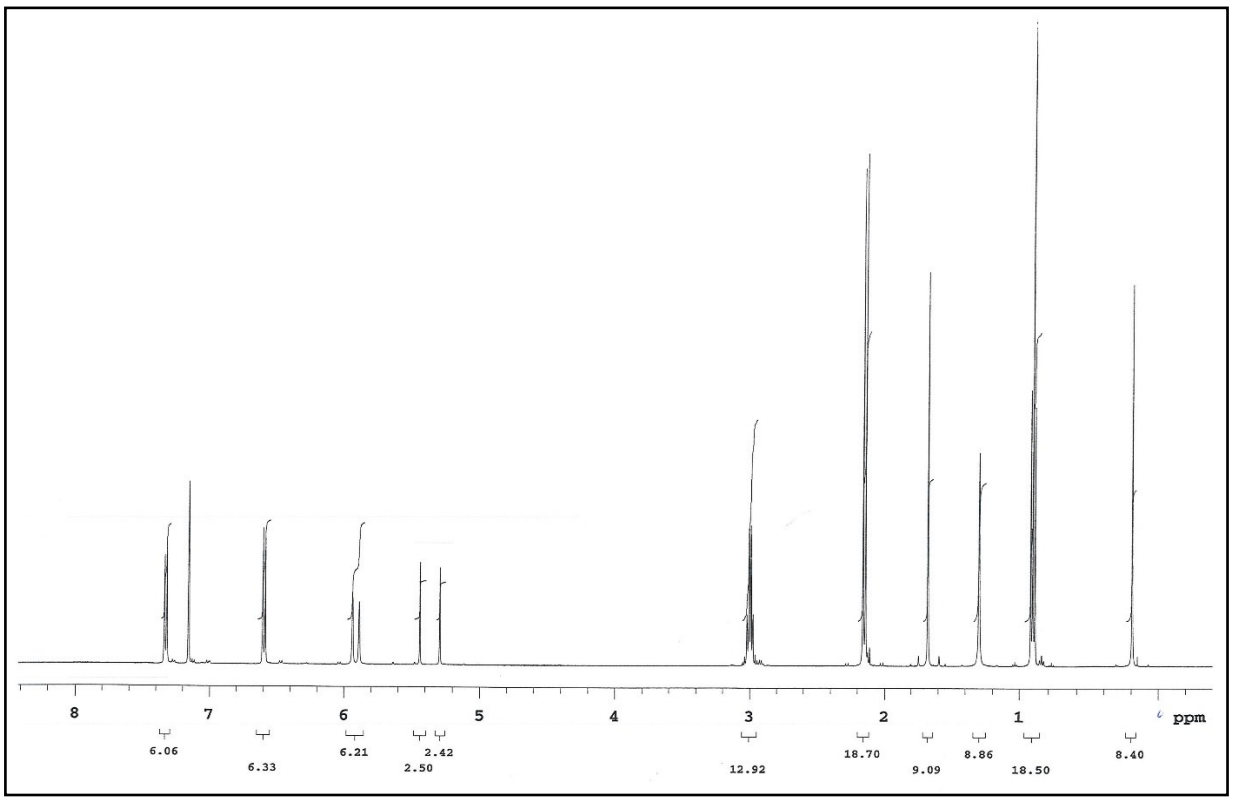

Figure S5a. ^{1}H NMR spectrum of complex [Zn(Me)(bpzaepe)] (**7**).

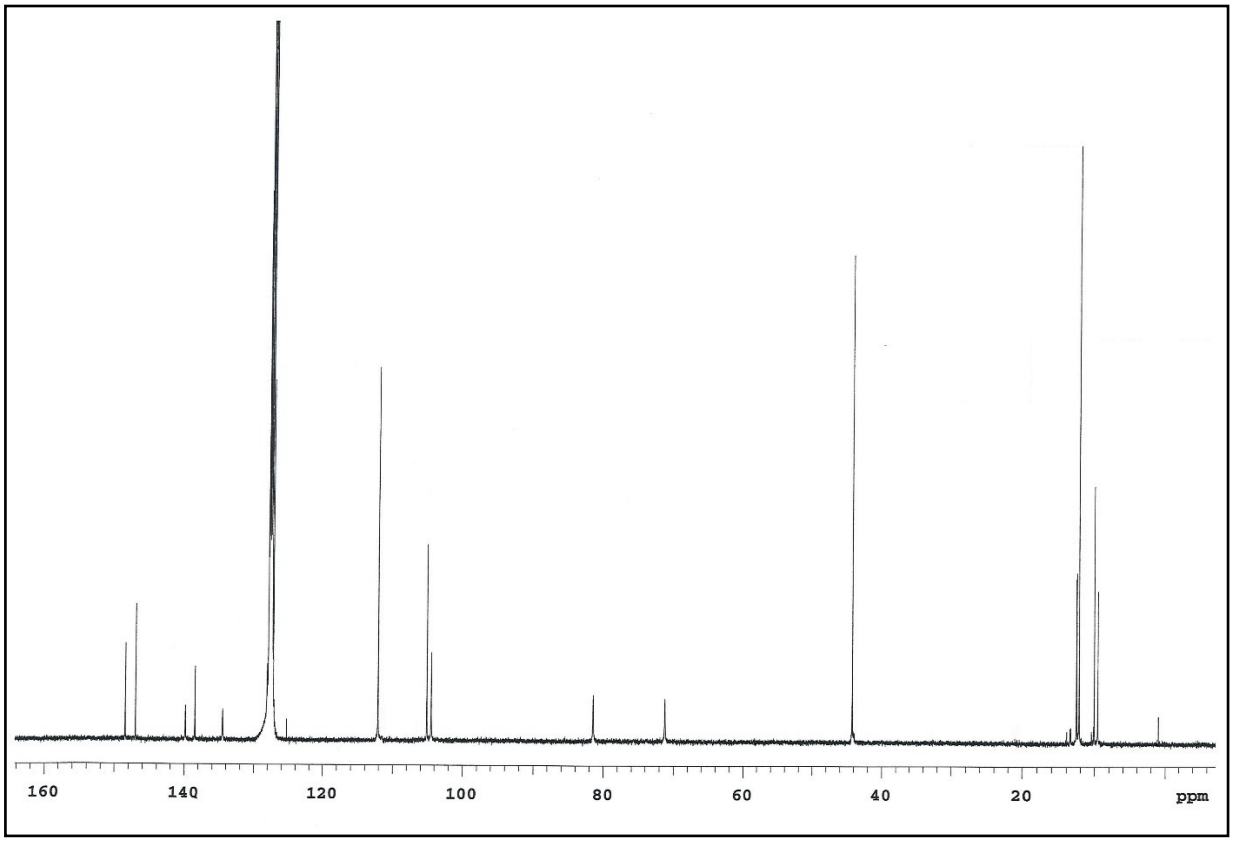

Figure S5b. $^{13}C\{^{1}H\}$ NMR spectrum of complex [Zn(Me)(bpzaepe)] (**7**).

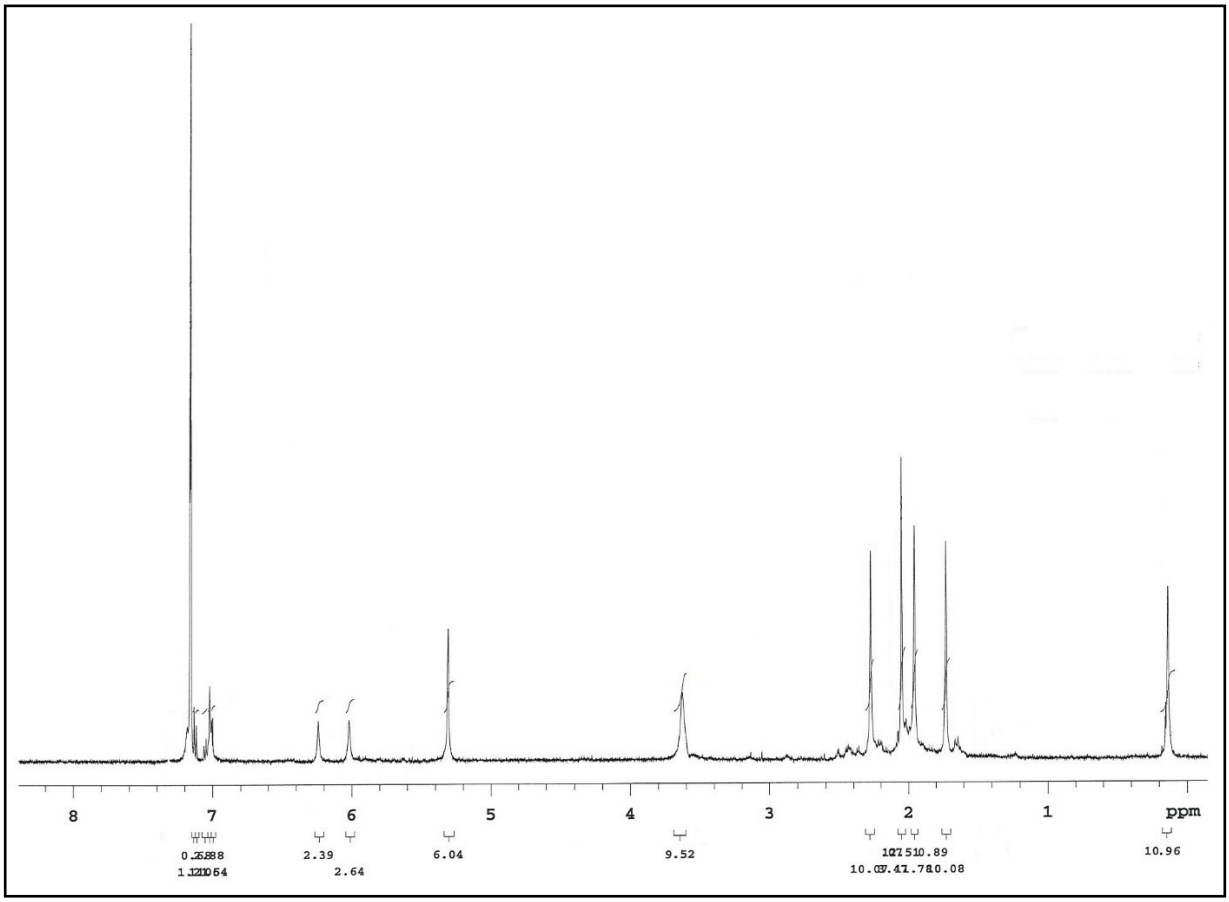

Figure S6a. ^{1}H NMR spectrum of complex [Zn(Me)(bpzime)] (**10**).

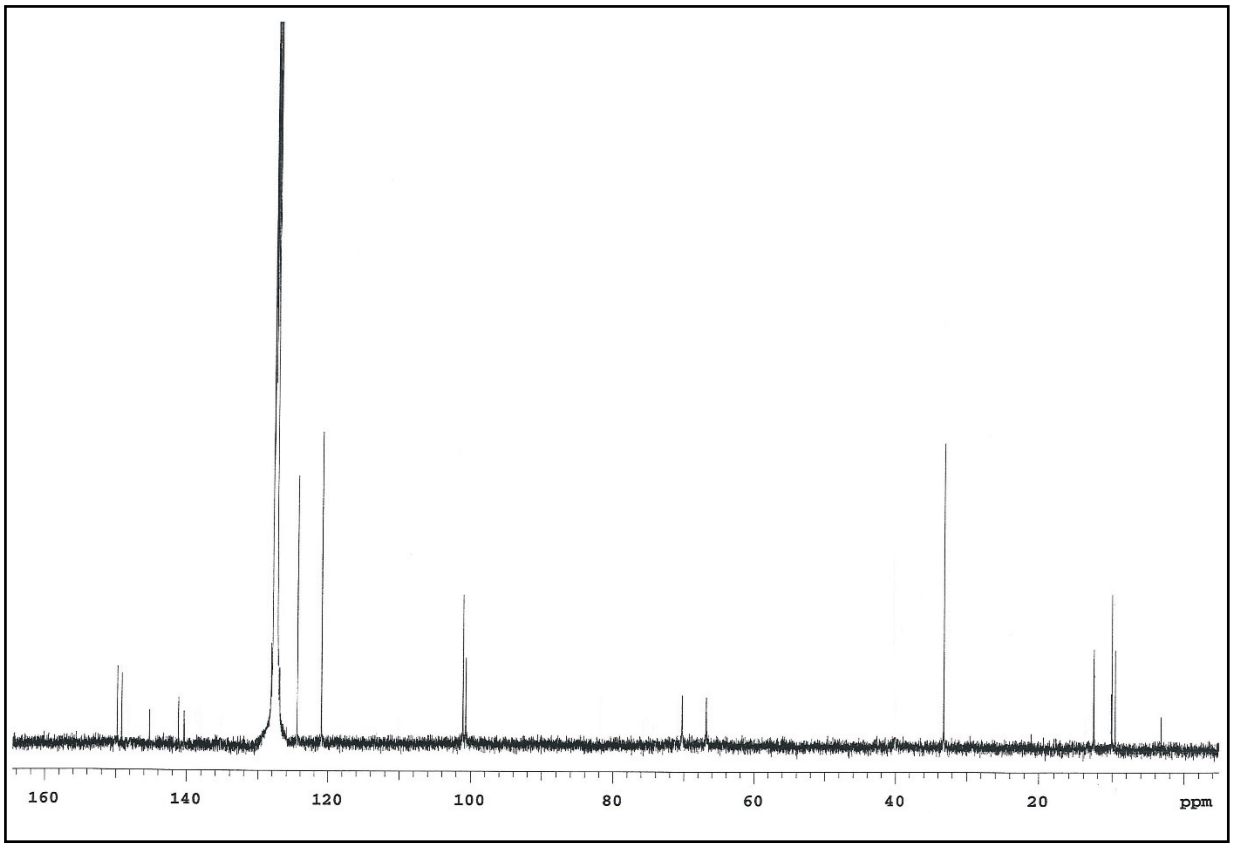

Figure S6b. ^{13}C{^{1}H} NMR spectrum of complex [Zn(Me)(bpzime)] (**10**).

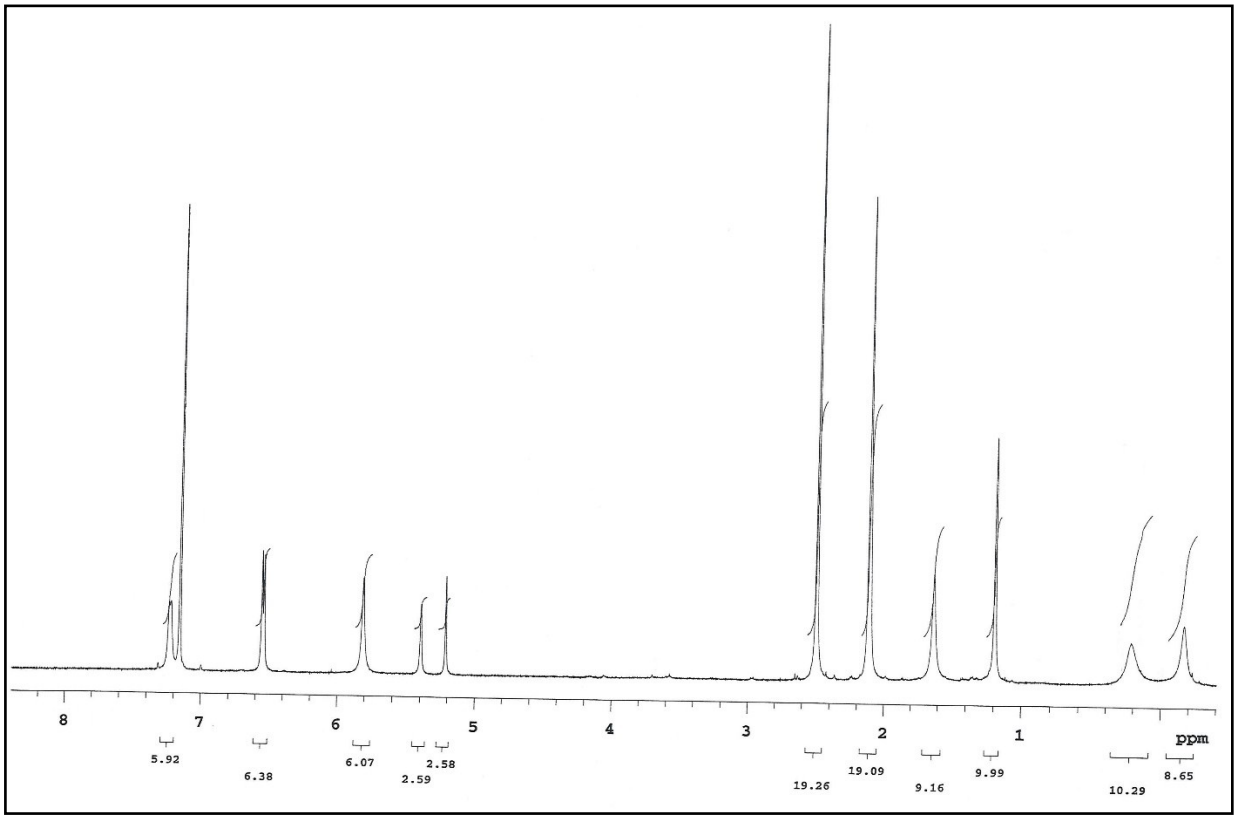

Figure S7a. ^{1}H NMR spectrum of complex [Zn(Me)(bpzampe)Zn(Me)$_2$] (**13**).

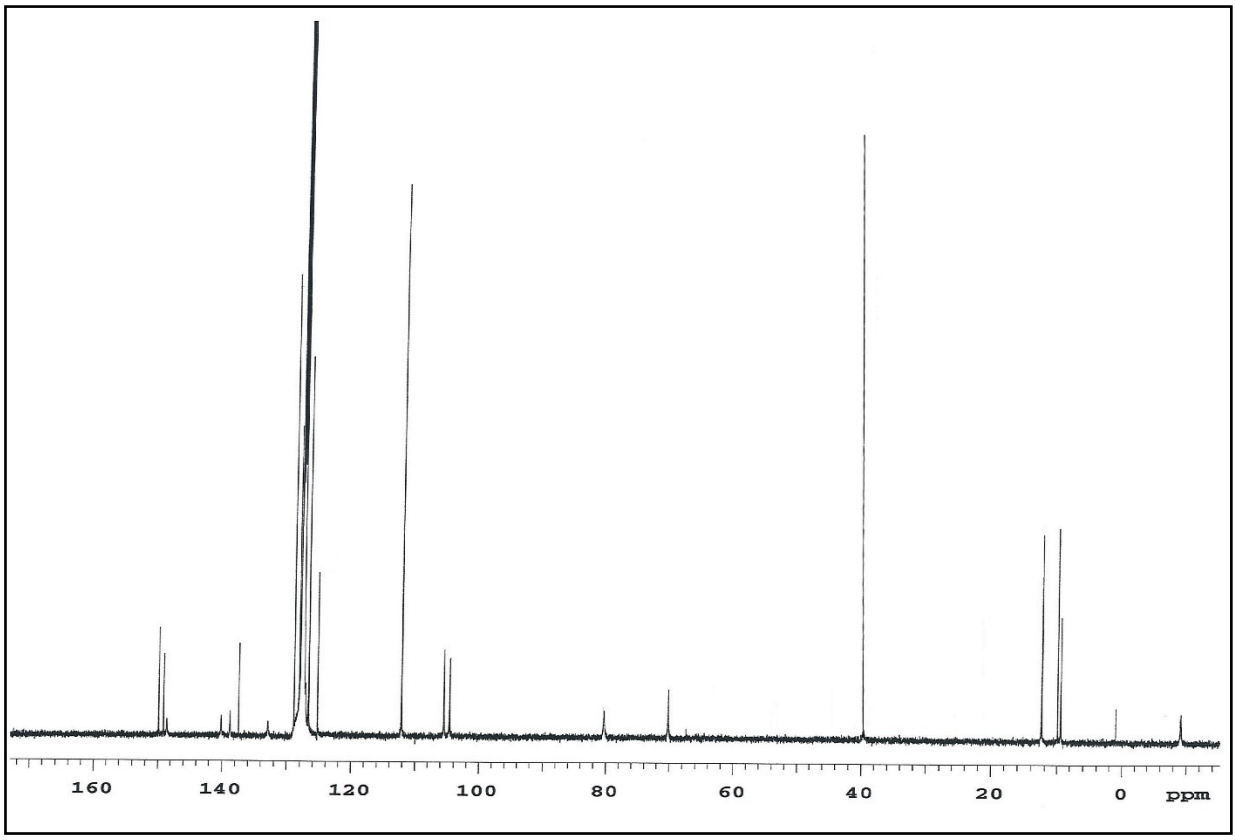

Figure S7b. $^{13}C\{^{1}H\}$ NMR spectrum of complex [Zn(Me)(bpzampe)Zn(Me)$_2$] (**13**).

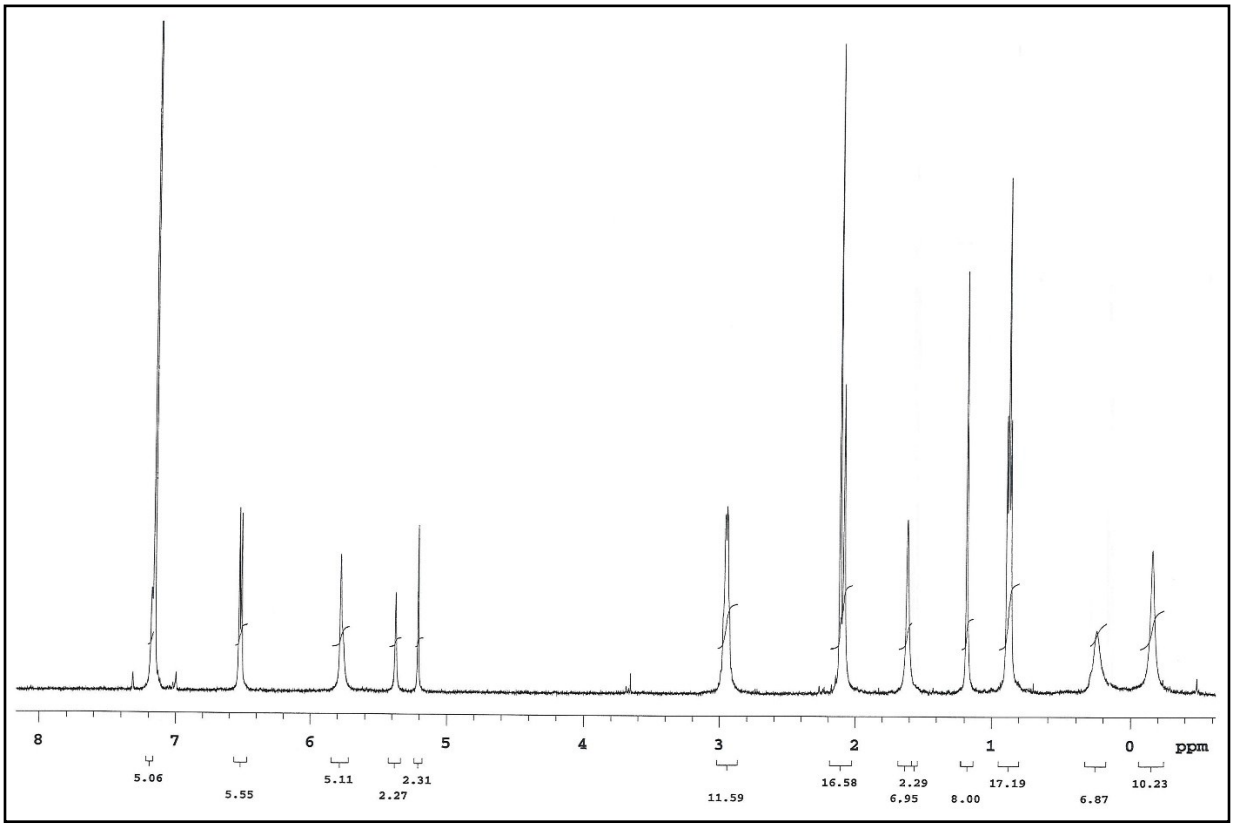

Figure S8a. ^{1}H NMR spectrum of complex [Zn(Me)(bpzaepe)Zn(Me)$_2$] (**15**).

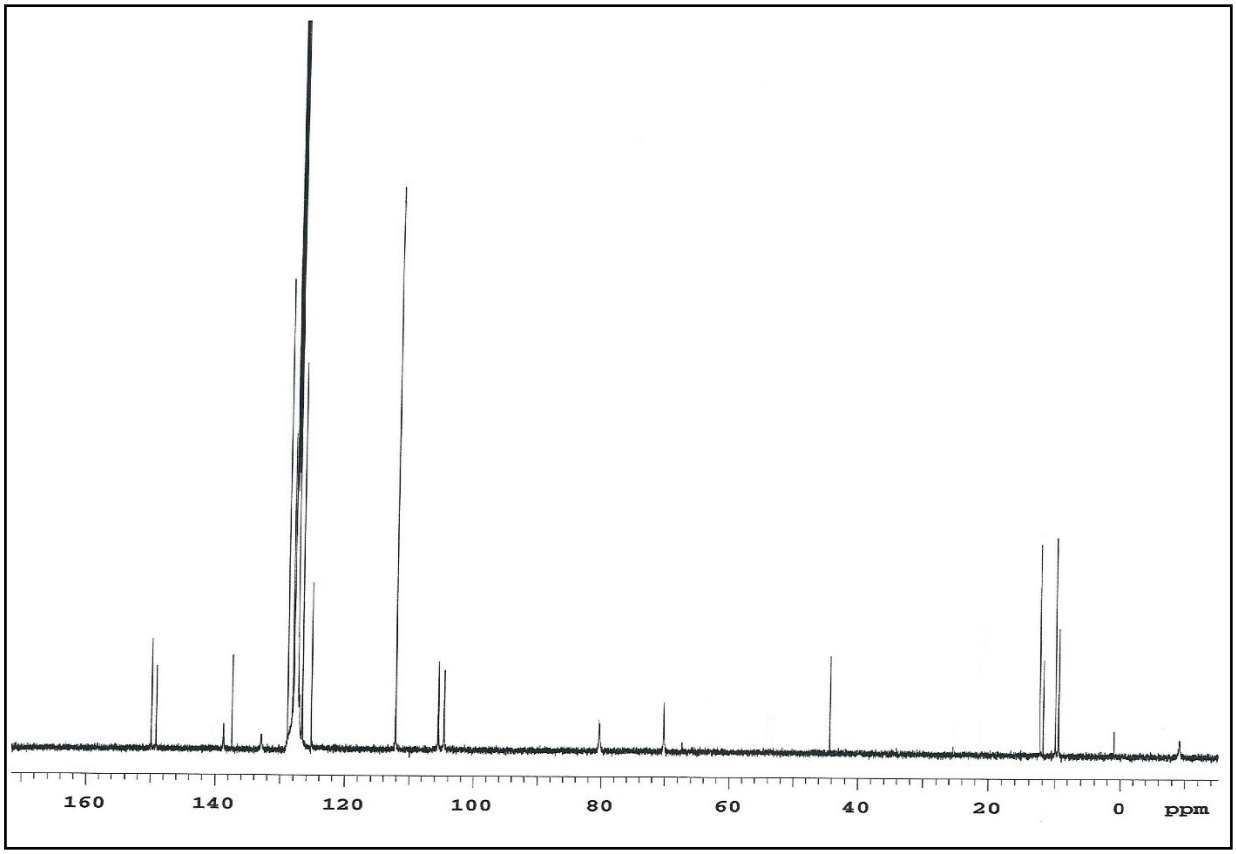

Figure S8b. $^{13}C\{^{1}H\}$ NMR spectrum of complex [Zn(Me)(bpzaepe)Zn(Me)$_2$] (**15**).

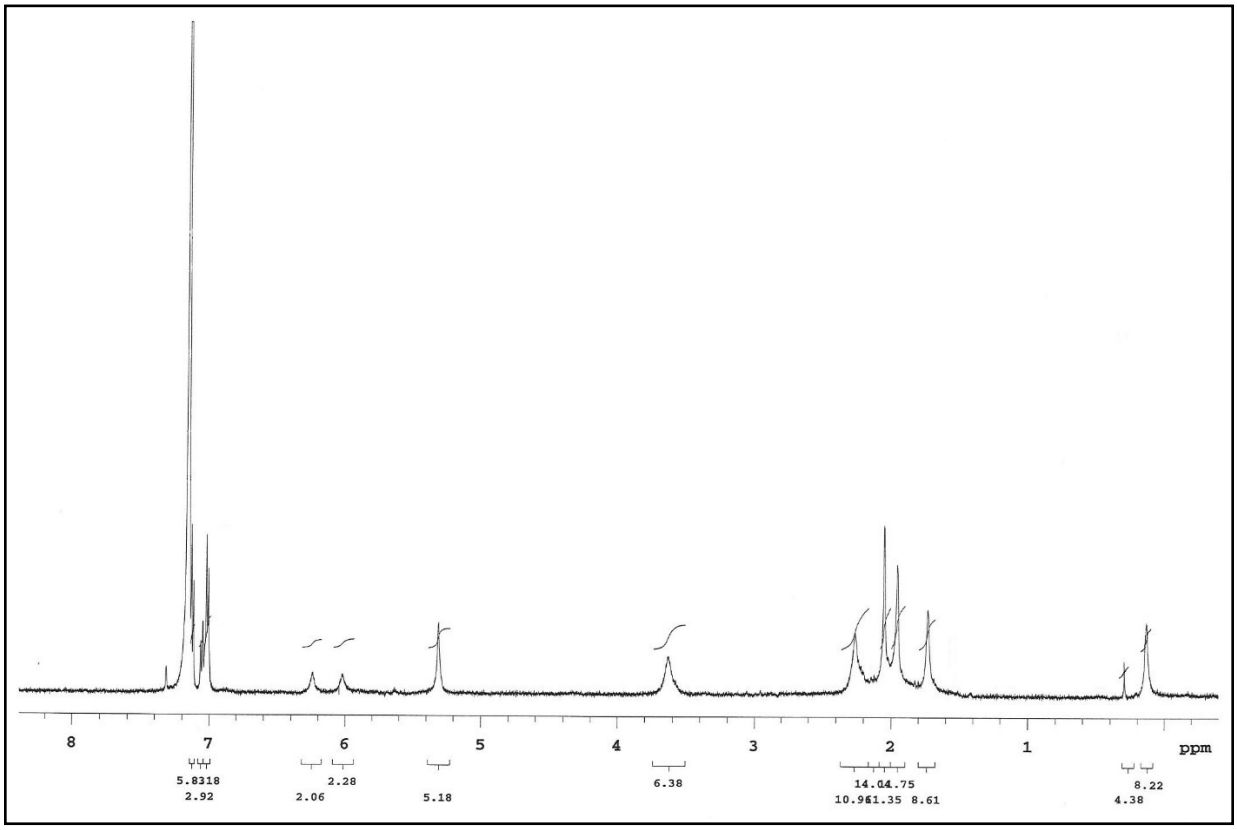

Figure S9a. ^{1}H NMR spectrum of complex [Zn(Me)(bpzime)Zn(Me)$_2$] (**17**).

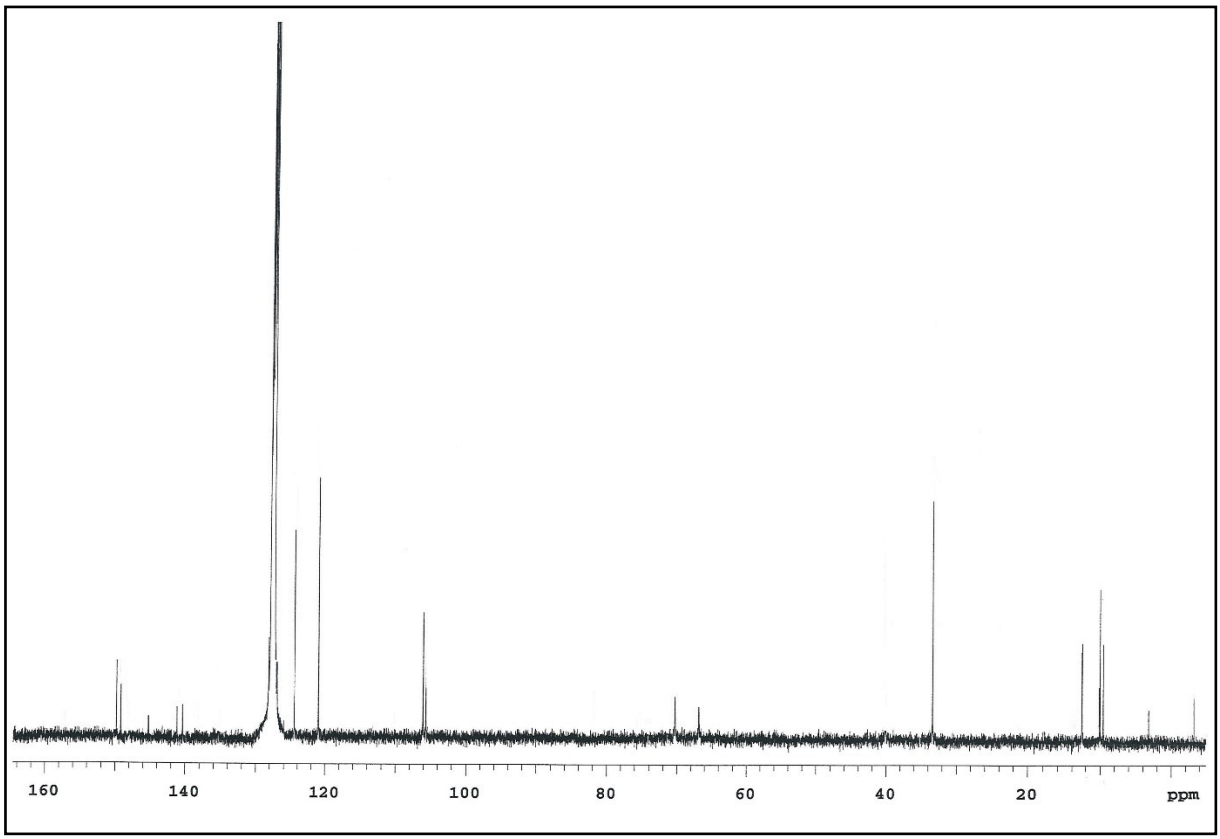

Figure S9b. $^{13}C\{^{1}H\}$ NMR spectrum of complex [Zn(Me)(bpzime)Zn(Me)$_2$] (**17**).

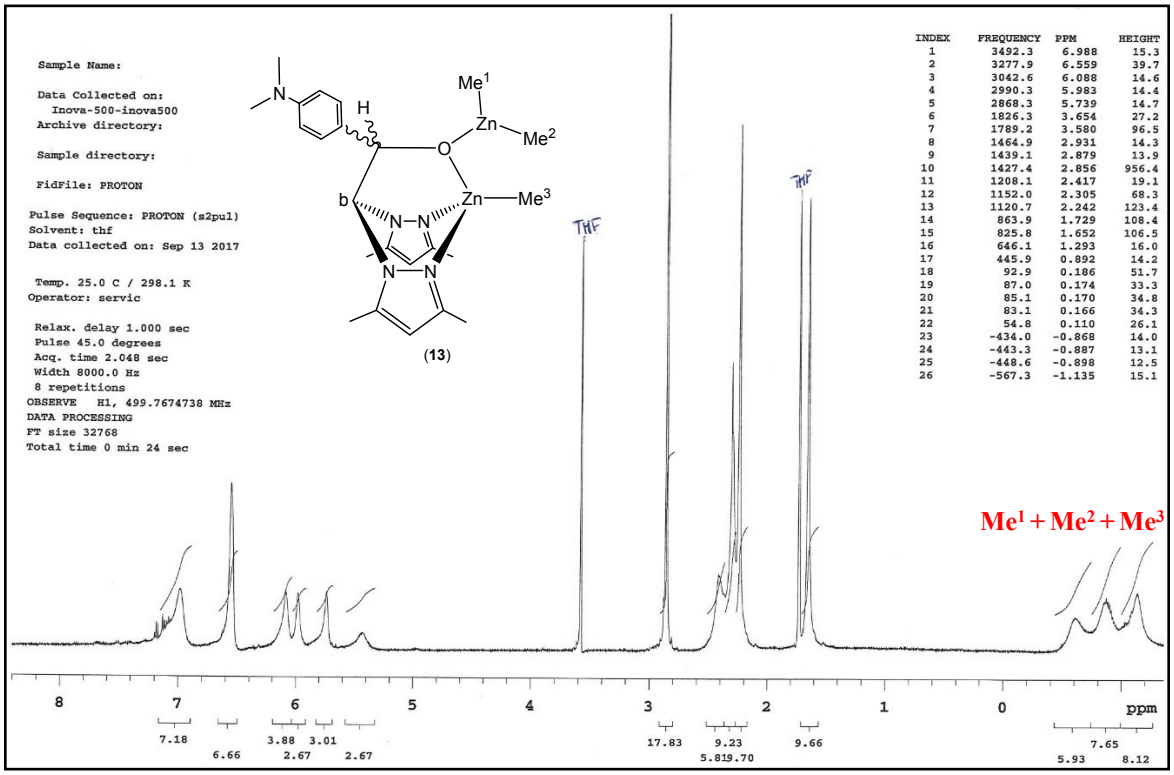

(a)

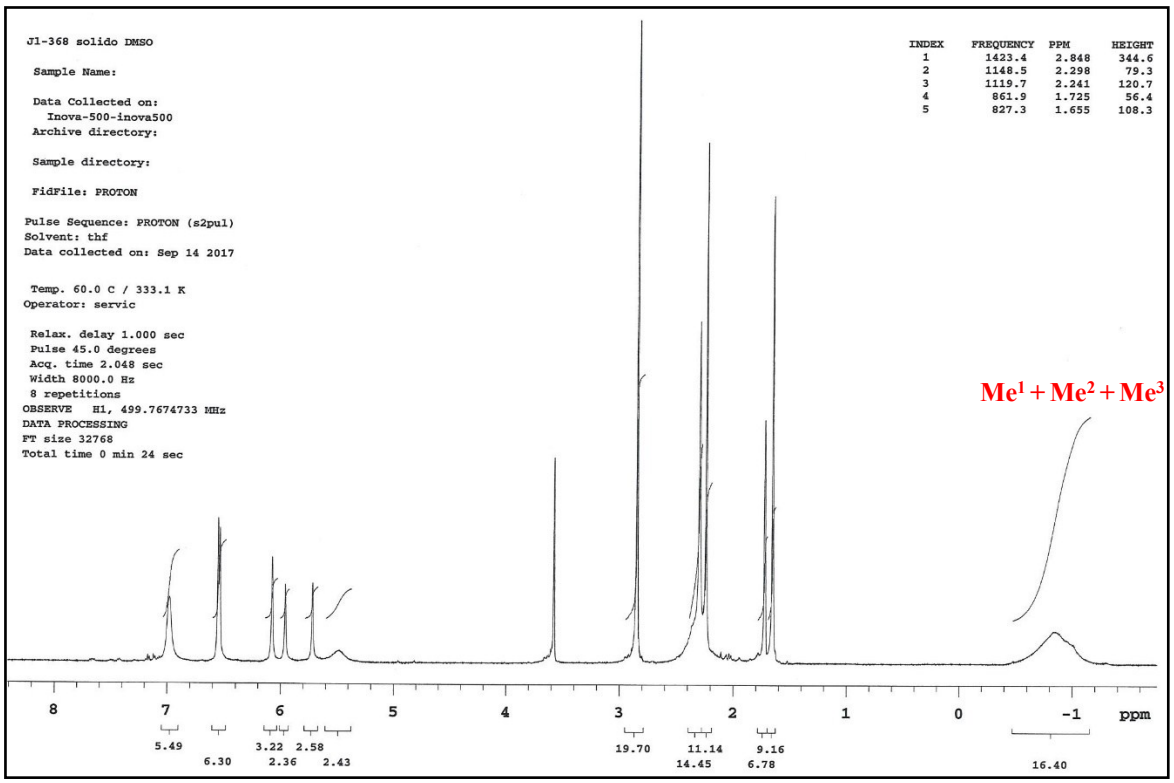

(b)

Figure S10. ^{1}H NMR spectra (thf-d_8) in the region of the methyl groups for complex [Zn(Me)(bpzampe)Zn(Me)$_2$] (**13**) at 25ºC (*a*) and 60ºC (*b*).

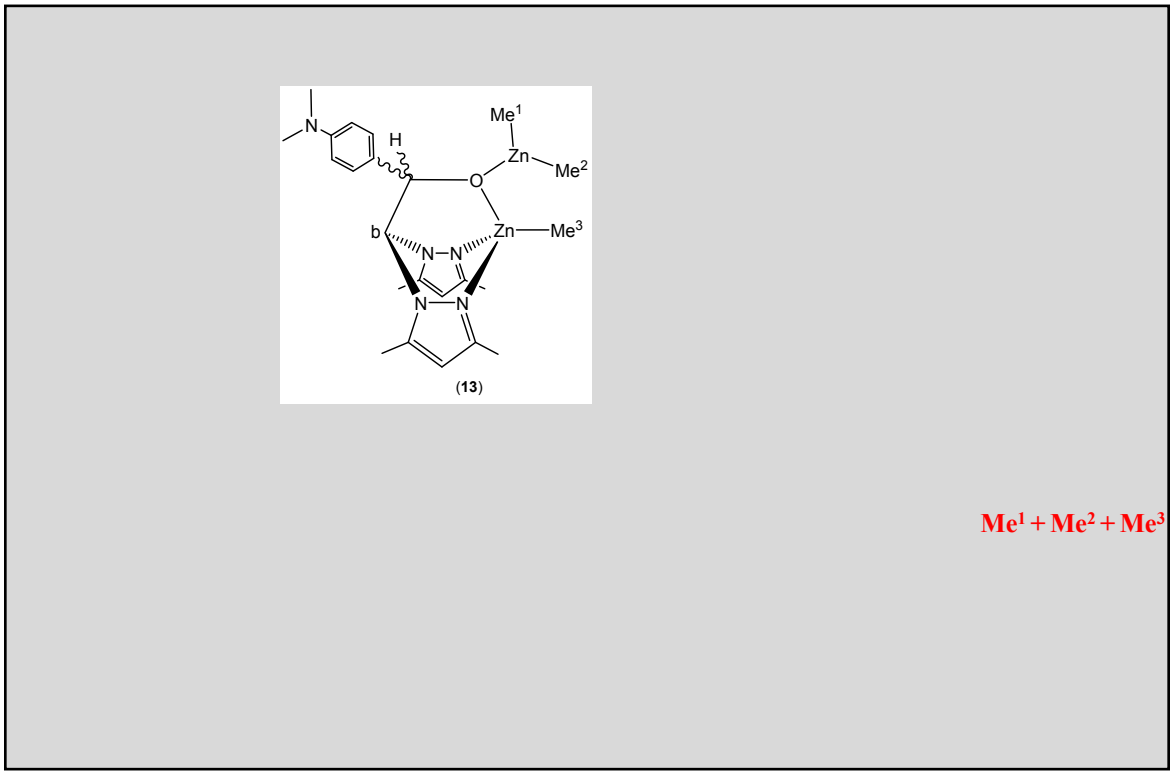

(a)

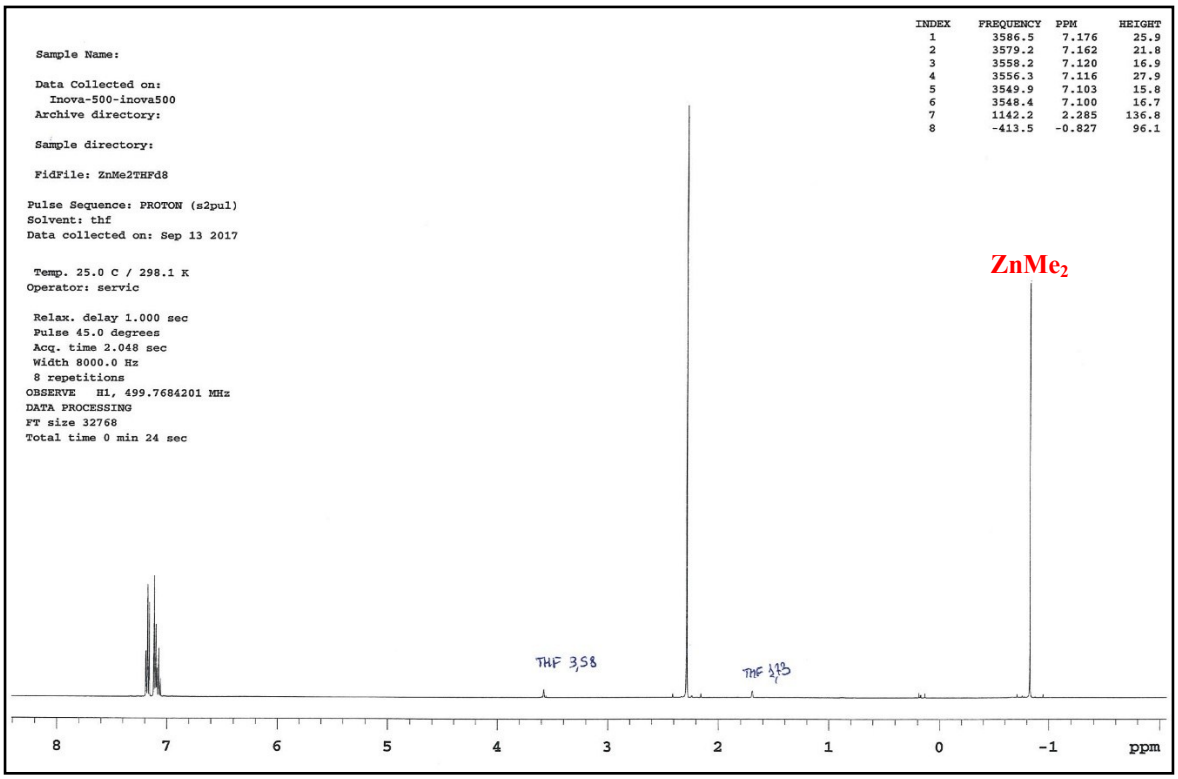

(b)

Figure S11. ^{1}H NMR spectra (thf-d_8, 25ºC) for complex [Zn(Me)(bpzampe)Zn(Me)$_2$] (**13**) (*a*) and commercial $ZnMe_2$ in toluene 2M (*b*).

22/05/2017 10:59:23 1 / 1

==== Shimadzu LCsolution Analysis Report ====

C:\LabSolutions\Data\gpcresultados\2016\Sonia\PLA03.lcd

Acquired by	: Admin
Sample Name	: PLA3
Sample ID	: PLA3
Vail #	:
Injection Volume	: 20 uL
Data File Name	: PLA03.lcd
Method File Name	: Calibrado2014.OK.lcm
Batch File Name	: SingleRun120160225171047.lcb
Report File Name	: Default.lcr
Data Acquired	: 25/02/2016 18:10:58
Data Processed	: 22/05/2017 10:45:24

<Chromatogram>

C:\LabSolutions\Data\gpcresultados\2016\Sonia\PLA03.lcd

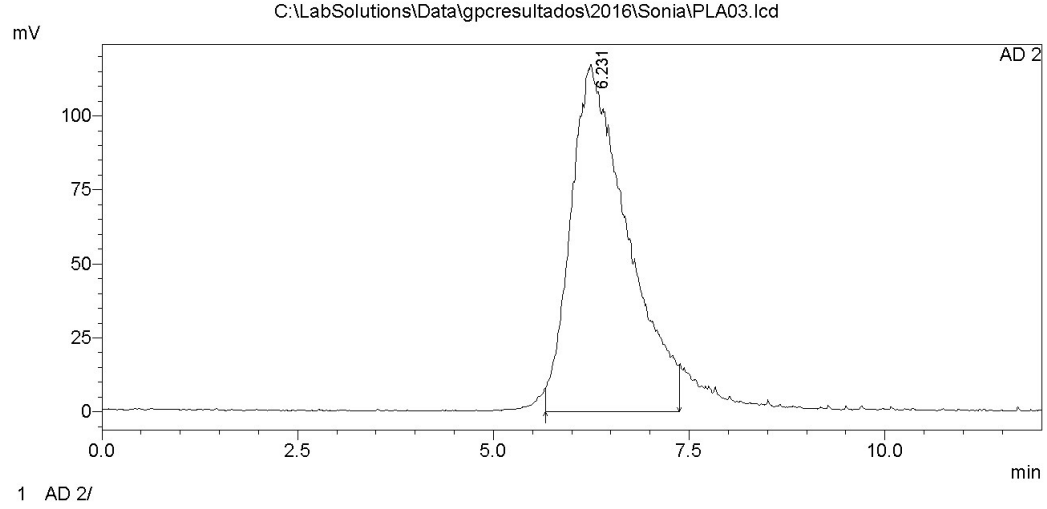

GPC Summary

Chromatogram AD 2

#	Title	Mn	Mw	Mv	Mw/Mn
1	PLA03.lcd	15914	17125	0	1.07608
	Average	15914	17125	0	1.07608
	%RSD	0.000	0.000	0.000	0.000
	Maximum	15914	17125	0	1.07608
	Minimum	15914	17125	0	1.07608
	SD	0	0	0	0.00000

Figure S12. GPC trace corresponding to a poly(*rac*-lactide) prepared from catalyst [Zn(Me)(bpzampe)Zn(Me)$_2$] (**13**) (Table 2, entry 20).

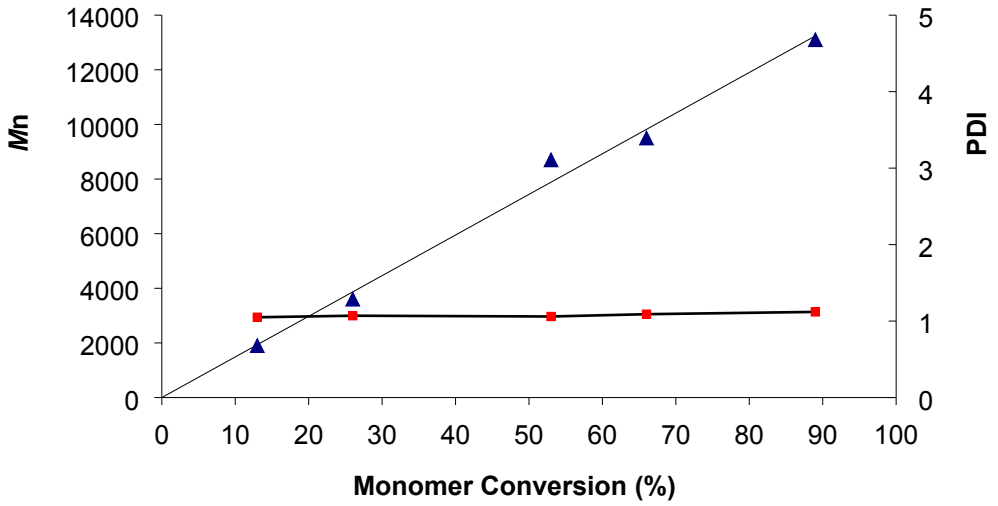

Figure S13. Plot of PLA M_n and molecular weight distribution values (PDI) as a function of monomer conversion (%) for the polymerization of *rac*-LA initiated by [Zn(Me)(bpzaepe)] (**7**); $[rac\text{-LA}]_0/[Zn]_0$ = 100, tetrahydrofuran, 20 ºC (Table 2, entries 6–10, R^2 = 0.993).

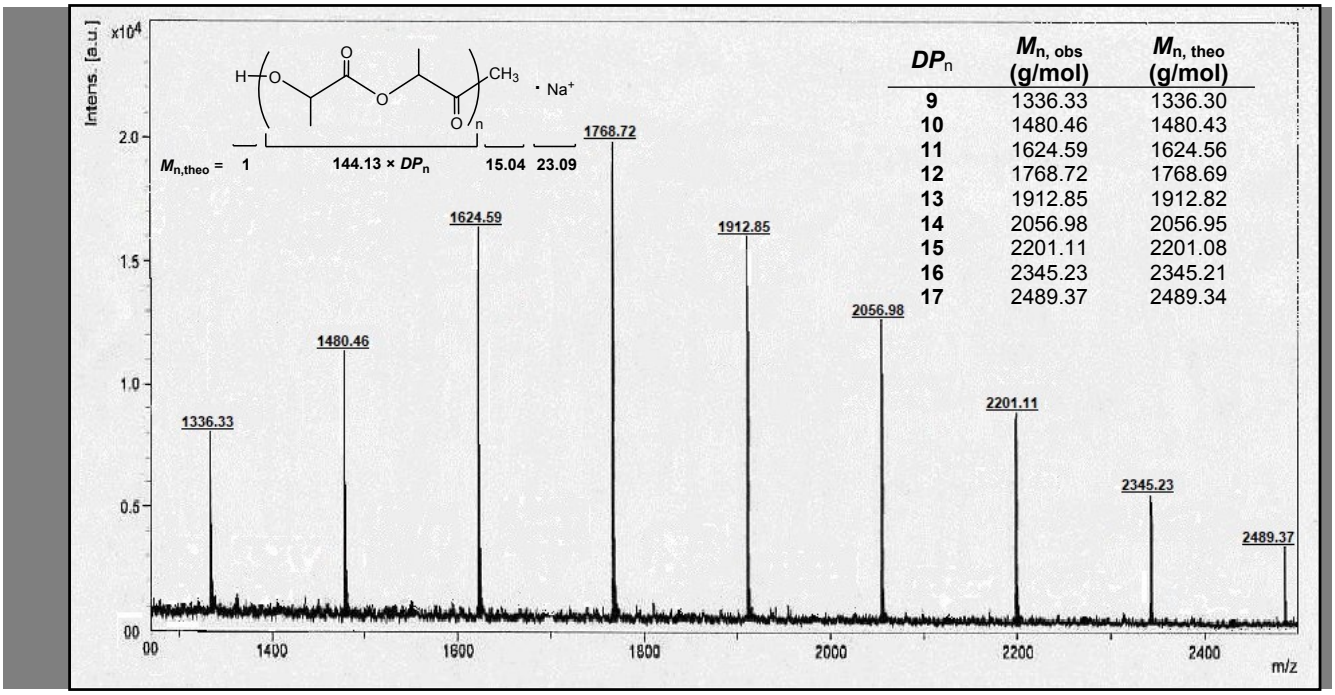

Figure S14a. Selected area of the MALDI-ToF mass spectrum of a PLA sample obtained on using initiator [Zn(Me)(bpzaepe)] (**7**) with [*rac*-LA]$_0$/[Zn]$_0$ = 20, 85% conversion; theoretical molecular weights calculated according to the equation: $M_n = (DP_n \times M_{wLA}) + M_{wMeH} + M_{wNa}$, where DP_n is the degree of polymerization, M_{wLA} = 144.13 g·mol^{-1}, M_{wMeH} = 16.04 g·mol^{-1} and M_{wNa} = 23.09 g·mol^{-1}.

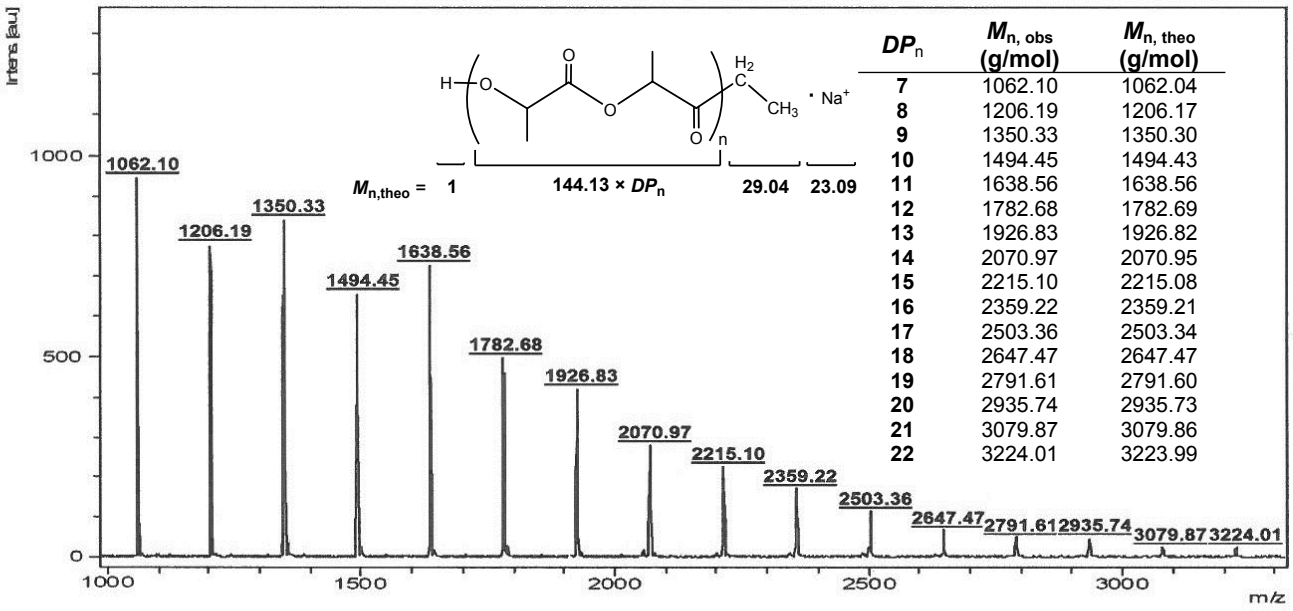

DP_n	$M_{n,obs}$ (g/mol)	$M_{n,theo}$ (g/mol)
7	1062.10	1062.04
8	1206.19	1206.17
9	1350.33	1350.30
10	1494.45	1494.43
11	1638.56	1638.56
12	1782.68	1782.69
13	1926.83	1926.82
14	2070.97	2070.95
15	2215.10	2215.08
16	2359.22	2359.21
17	2503.36	2503.34
18	2647.47	2647.47
19	2791.61	2791.60
20	2935.74	2935.73
21	3079.87	3079.86
22	3224.01	3223.99

Figure S14b. Selected area of the MALDI-ToF mass spectrum of a PLA sample obtained on using initiator [Zn(Et)(bpzaepe)] (**8**) with [*rac*-LA]$_0$/[Zn]$_0$ = 30, 73% conversion; theoretical molecular weights calculated according to the equation: $M_n = (DP_n \times M_{wLA}) + M_{wEtH} + M_{wNa}$, where DP_n is the degree of polymerization, M_{wLA} = 144.13 g·mol^{-1}, M_{wEtH} = 30.04 g·mol^{-1} and M_{wNa} = 23.09 g·mol^{-1}.

The distribution in the spectrum indicates the existence of a single family of polymer chains capped by –CH(CH$_3$)OH, and (CH$_3$–OC(O)– and (CH$_3$–CH$_2$–OC(O)– *termini* for **7** and **8**, respectively, corresponding to oligomers of formula H(OCHMeCO)$_{2n}$(CH$_3$)·Na$^+$ (n = 9 to 17) and H(OCHMeCO)$_{2n}$(CH$_2$–CH$_3$)·Na$^+$ (n = 7 to 22), respectively, with consecutive peaks separated by increments of 144 Da (Figure S13a and S13b, respectively). Moreover, neither intermolecular ester-exchange (transesterification) reactions nor cyclic oligomers were detected.

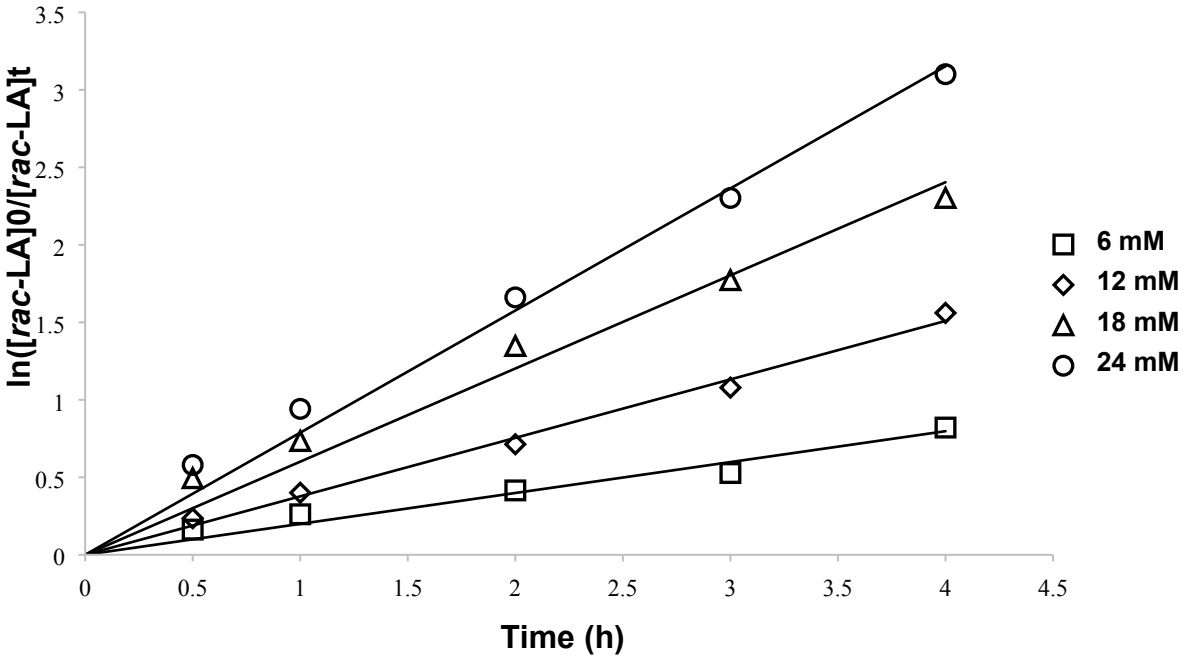

Figure S15. Pseudo-first-order kinetic plots for the polymerization of *rac*-LA in tetrahydrofuran at 20ºC employing [Zn(Me)(bpzaepe)] (**7**) as catalyst ($[rac\text{-LA}]_0$ = 0.80 M).

In all cases, the linearity of the semi-logarithmic plot of ln ($[rac\text{-LA}]_0/[rac\text{-LA}]_t$) versus reaction time for catalyst **7** at 20ºC, employing different initial catalyst concentrations, shows that the propagations were first order with respect to *rac*-LA monomer (Figure S14) (square correlation coefficients ≥ 0.97).

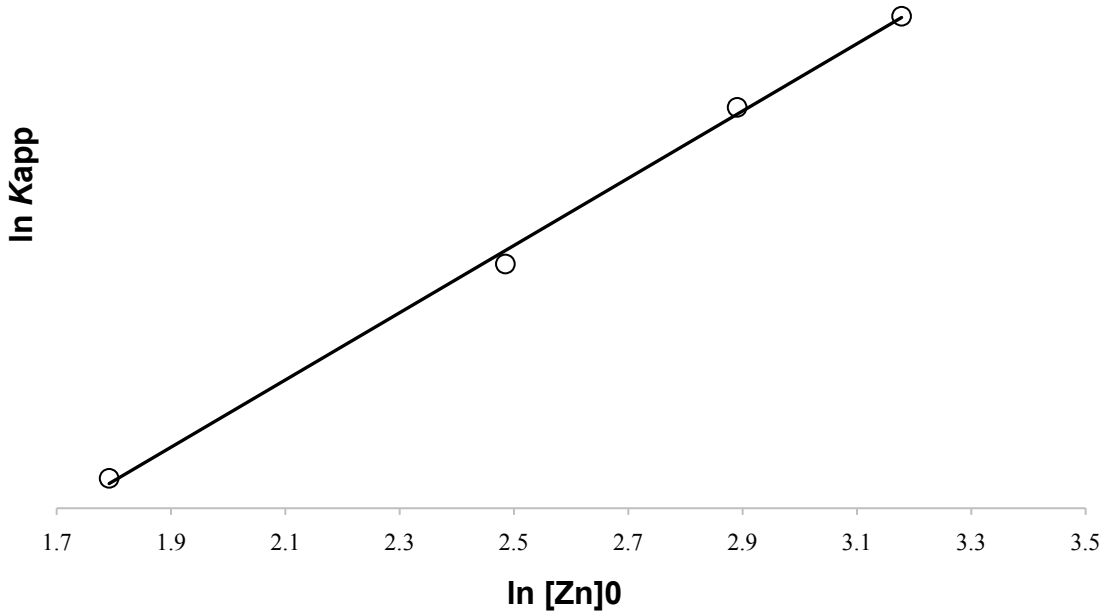

Figure S16. Plot of ln k_{app} versus ln [catalyst]$_0$ for the polymerization of *rac*-LA employing initiator [Zn(Me)(bpzaepe)] (**7**) in tetrahydrofuran at 20ºC, with [*rac*-LA]$_0$ = 0.75 mol/L.

The kinetic dependence on the catalyst concentration (n) and the propagation rate constant (k_p) confirms that the reaction is also first order in catalysts **7** at 20ºC (Figure S15). These values prove that the polymerization of *rac*-LA mediated by this initiator obeys an overall second-order rate kinetic law of the form:

$$-d[rac\text{-LA}]/dt = k_p[\text{catalyst}]^1[rac\text{-LA}]^1$$

Table S1. Rate constants dependence on the initial concentration of [Zn(Me)(bpzaepe)] (**7**) for *rac*-LA polymerization at 20ºC.

$[catalyst]_0 \times 10^3$ (M)	$k_{app} \times 10^5$ (s^{-1})	$k_p \times 10^3$ ($M^{-1} \cdot s^{-1}$)	*n*
8	5.5 ± 0.3	8.5 ± 0.6	1.04 ± 0.03
12	11.1 ± 0.2		
18	16.7 ± 0.7		
20	23.7 ± 0.8		

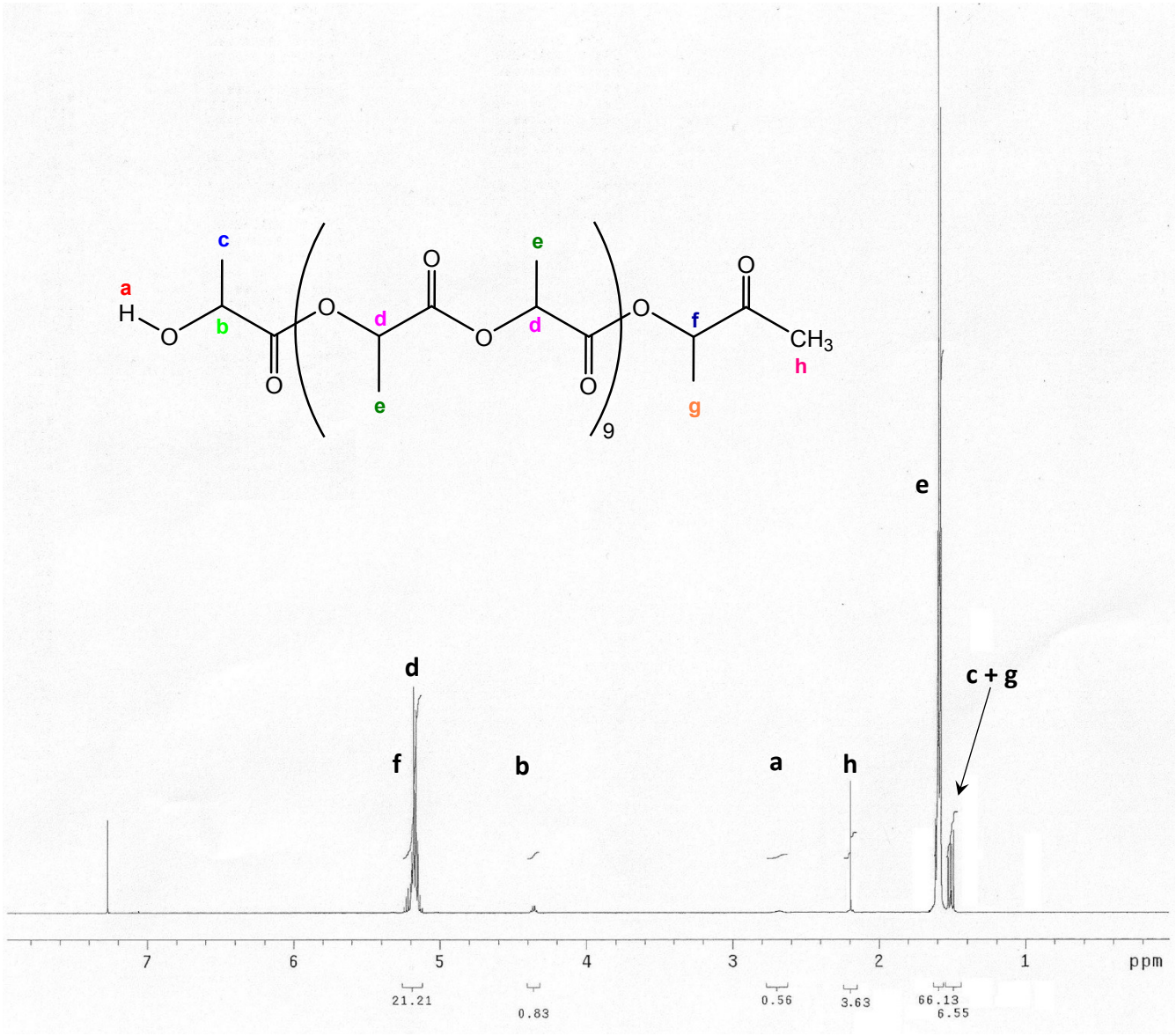

Figure S17. ^{1}H NMR spectrum (400 MHz, 298 K, $CDCl_3$) of PLA prepared by the polymerization of *rac*-LA initiated by [Zn(Me)(bpzaepe)] (**7**) at 67% of conversion showing all resonances and assignments, including the chain *termini* ($[rac\text{-LA}]_0/[Zn]_0 = 15$, tetrahydrofuran, 20 ºC).

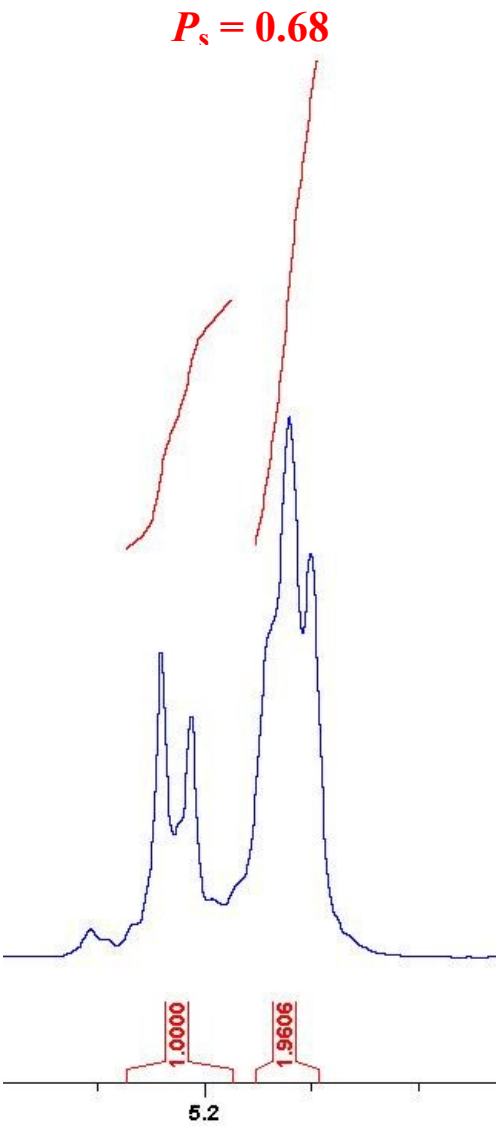

Figure S18. ^{1}H NMR spectrum (400 MHz, 298 K, $CDCl_3$) of the homodecoupled C*H* resonance of poly(*rac*-lactide) prepared employing [Zn(Me)(bpzaepe)] (**7**) in tetrahydrofuran at 0ºC for 24 h (Table 2, entry 5). The tacticity of the polymer was assigned using the methine signals with homonuclear decoupling, as described by Hillmyer and co-workers.[1]

Table S2. Crystal data and structure refinement for **4** and **5**.

	4	**5**
Empirical formula	C_{21} H_{29} N_5 O Zn	C_{22} H_{31} N_5 O Zn
Formula weight	432.86	446.89
Temperature (K)	240(2)	240(2)
Wavelength (Å)	0.71073	0.71073
Crystal system	Monoclinic	Monoclinic
Space group	P 2_1/c	P 2_1/c
a(Å)	13.201(3)	12.951(3)
b(Å)	15.952(3)	16.222(4)
c(Å)	10.310(2)	10.789(3)
β(°)	91.966(3)	92.045(4)
Volume(Å^3)	2169.9(7)	2265.1(10)
Z	4	4
Density (calculated) (g/cm^3)	1.325	1.310
Absorption coefficient (mm^{-1})	1.152	1.106
F(000)	912	944
Crystal size (mm^3)	0.28 x 0.18 x 0.12	0.21 x 0.15 x 0.09
Index ranges	$-15 \le h \le 15$ $-18 \le k \le 17$ $-12 \le l \le 12$	$-15 \le h \le 15$ $-14 \le k \le 19$ $-12 \le l \le 12$
Reflections collected	14175	13960
Independent reflections	3822 [R(int) = 0.0533]	3981 [R(int) = 0.1269]
Data / restraints / parameters	3822 / 0 / 260	3981 / 0 / 262
Goodness-of-fit on F^2	1.020	0.959
Final R indices [$I>2\sigma(I)$]	R1 = 0.0419, wR2 = 0.0933	R1 = 0.0583, wR2 = 0.1201
Largest diff. peak / hole, e.Å^{-3}	0.258 / -0.310	0.339 / -0.345

[a] $R = \Sigma||F_o|-|F_c|/\Sigma|F_o|$. [b] $wR = \{\Sigma w(F_o^2-F_c^2)^2/\Sigma w(F_o^2)^2\}^{1/2}$. [c] GOF = $\{\Sigma\ [w((F_o^2-F_c^2)^2)/(n-p)\}^{1/2}$, where n = number of reflections and p = total number of parameters refined.

References

(1) M. T. Zell, B. E. Padden, A. J. Paterick, K. A. M. Thakur, R. T. Kean, M. A. Hillmyer, E. J. Munson, *Macromolecules*, 2002, **35**, 7700–7707.